ARL-TR-9402 ● FEB 2022

DEVCOM ARMY RESEARCH LABORATORY

Modeling the Electrical Conductivity of Thermally Ionized Air Produced in Normal Shock Waves at Hypersonic and Hypervelocity Speeds

by Sergei Izvekov and Robert L Doney

NOTICES

Disclaimers

The findings in this report are not to be construed as an official Department of the Army position unless so designated by other authorized documents.

Citation of manufacturer's or trade names does not constitute an official endorsement or approval of the use thereof.

Destroy this report when it is no longer needed. Do not return it to the originator.

ARL-TR-9402 ● FEB 2022

Modeling the Electrical Conductivity of Thermally Ionized Air Produced in Normal Shock Waves at Hypersonic and Hypervelocity Speeds

Sergei Izvekov and Robert L Doney
US Army Combat Capabilities Development Command
Army Research Laboratory

REPORT DOCUMENTATION PAGE

Form Approved
OMB No. 0704-0188

1. REPORT DATE *(DD-MM-YYYY)*	2. REPORT TYPE	3. DATES COVERED (From - To)
February 2022	Technical Report	10 January 2021–30 September 2022

4. TITLE AND SUBTITLE
Modeling the Electrical Conductivity of Thermally Ionized Air Produced in Normal Shock Waves at Hypersonic and Hypervelocity Speeds

5a. CONTRACT NUMBER

5b. GRANT NUMBER

5c. PROGRAM ELEMENT NUMBER

6. AUTHOR(S)
Sergei Izvekov and Robert L Doney

5d. PROJECT NUMBER

5e. TASK NUMBER

5f. WORK UNIT NUMBER

7. PERFORMING ORGANIZATION NAME(S) AND ADDRESS(ES)
DEVCOM Army Research Laboratory
ATTN: FCDD-RLW-WA
Aberdeen Proving Ground, MD 21005

8. PERFORMING ORGANIZATION REPORT NUMBER
ARL-TR-9402

9. SPONSORING/MONITORING AGENCY NAME(S) AND ADDRESS(ES)

10. SPONSOR/MONITOR'S ACRONYM(S)

11. SPONSOR/MONITOR'S REPORT NUMBER(S)

12. DISTRIBUTION/AVAILABILITY STATEMENT
Approved for public release: distribution unlimited.

13. SUPPLEMENTARY NOTES
ORCID ID: Sergei Izvekov, 0000-0003-4755-9138

14. ABSTRACT
In this report, we model the electronic conductivity of low-temperature plasma formed due to thermal ionization of dry air in normal shock waves at hypersonic and hypervelocity Mach numbers (6–30 km s_{-1}) using the multiterm Boltzmann equation, Monte Carlo collision, and Cheetah 9.0 equation of state methods.

15. SUBJECT TERMS
electrical conductivity, plasma, hypersonic air flow, normal shock wave, Mach number, Boltzmann equation, Monte Carlo collision

16. SECURITY CLASSIFICATION OF:			17. LIMITATION OF ABSTRACT	18. NUMBER OF PAGES	19a. NAME OF RESPONSIBLE PERSON
a. REPORT	b. ABSTRACT	c. THIS PAGE			Sergei Izvekov
Unclassified	Unclassified	Unclassified	UU	34	19b. TELEPHONE NUMBER (Include area code) (410) 306-0720

Standard Form 298 (Rev. 8/98)
Prescribed by ANSI Std. Z39.18

Contents

List of Figures

List of Tables

Acknowledgments

The authors wish to thank Drs. Brian Barnes and Betsy Rice of the US Army Combat Capabilities Development Command Army Research Laboratory for their helpful comments. We also thank Ms. Jenny Weathers for her editorial review of this report.

This work was supported in part by a grant of computer time from the DOD High Performance Computing Modernization Program at the US Navy and DEVCOM Army Research Laboratory DOD Supercomputing Resource Centers.

1. Introduction

Hypersonic entry into the atmosphere generates very strong shock waves in the flow of surrounding air.[1] The extreme thermodynamic conditions produced by these shocks lead to real gas effects, such as internal energy excitation, ionization and recombination processes, and chemical reactions.[2,3] These processes may lead to the creation of electrically conductive plasma behind a normal shock wave (Fig. 1), which may affect important operational aspects of hypersonic vehicles. The knowledge of accurate electrical conductance properties of plasma formed in the shock-heated air in a broad range of the shock (upstream) Mach numbers (M_1)[4] is of fundamental importance to various other research areas relevant to existing and future research programs at the US Army Combat Capabilities Development Command Army Research Laboratory. One area of particular importance is further enhancement of critical DEVCOM Army Research Laboratory multiphysics modeling tools and requisite material models that require knowledge of electronic transport in the thermally ionized plasmas formed in shocked gases. Currently, the available experimental measurements are limited to a narrower range of M_1. In the absence of reliable experimental data on the ionization processes and charge transport in the shocked gases, theoretical techniques can provide crucial insight.

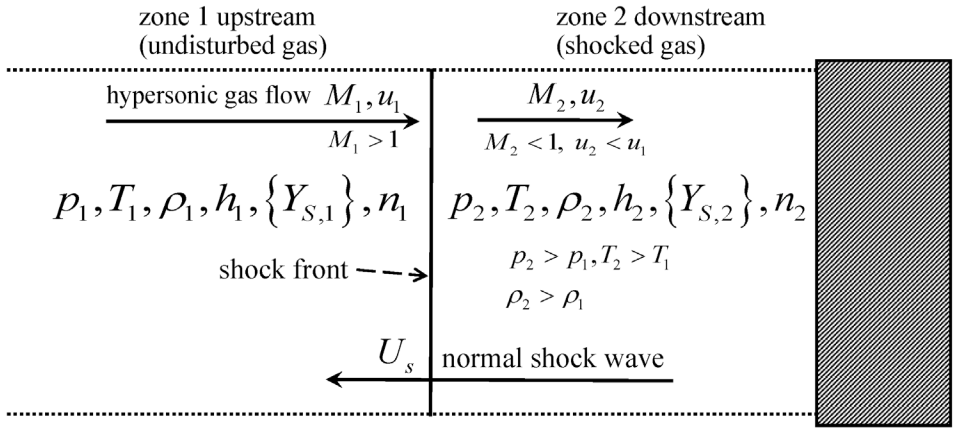

Fig. 1 Notation for normal shock wave: $M_i = u_i/a_i$ is Mach number, u_i is flow velocity (a_i is speed of sound), p_i is pressure, T_i is temperature, ρ_i is density ($1/\rho_i$ is specific volume v_i), h_i is enthalpy, $\{Y_{S,i}\}$, where S denotes a type of neutral or ionic specie, is chemical composition (molar fraction of neutrals and ions), n_i is a mole fraction of free electrons e^- (we assume $n_1 = 0$ and $n_2 = n/N$, where n is e^- density and N is plasma background density), and U_s is the normal shock wave velocity. Upstream Mach number M_1 is called shock Mach number (often denoted as M_s) because $M_1 = U_s/a_1$.

A key parameter in the research of ionization and charge transport in shock waves in reactive gases such as shocked air mixtures or gaseous detonation products[5–7] is the DC conductivity, or simply electrical conductivity (EC), σ, which depends on the thermodynamic conditions, chemical composition, and electron transport properties of the air plasma behind a normal shock wave.[1,8,9] The EC due to ionization and reactions occurring behind the fronts of gaseous shock waves has received relatively scant attention in comparison with the electrical conductance and ionization phenomena that occur in flames. The main reason for the lack of accurate quantitative experimental data is attributable to the difficulties encountered in measuring them—owing to the fast rates of reactions[2,3,10] and extreme thermodynamic conditions that occur behind shock waves. The EC of shock-heated air in the 3500–6200 K temperature range (which corresponds to hypersonic and hypervelocity flows with M_1 in the range of 8–18) and at densities on the order of 0.01 times normal temperature pressure (NTP) conditions, has been measured using the shock-tube technique.[10,11] These measurements indicated that the ionization builds up quickly behind the shock front and approaches the equilibrium value. This is supported by the fact that the measured σ agrees quite well with the calculated values based on the equilibrium degree of ionization and equilibrium electron transport properties.[2,11] It was suggested that for $M_1 \leq 27$ (~9.3 km s^{-1}), the predominant ionization mechanism is associative ionization (AI): $N + O = NO^+ + e^-$, $N + N = N_2^+ + e^-$, and $O + O = O_2^+ + e^-$; however, for higher M_1, electron impact becomes the predominant ionization mechanism.[3,12,13] The free electrons (e^-) and atomic/molecular ions produced by AI introduce new reaction mechanisms that complicate the physics and chemistry of the shock response of air. To be predictive of experimental results over a possibly wider range of M_1, EC models of shocked-air mixtures need to incorporate a thermodynamically consistent production of ionic species, chemical reactions due to charge-neutral and charge-charge interactions, the removal of charged species by recombination, and free electron elastic and inelastic scatterings caused by collisions with neutrals and ions. Such models can be based on ab initio or semi-empirical thermochemical equation of state (EOS) calculations to determine the air plasma composition behind normal shock waves combined with kinetic approaches to obtain the charge transport properties.

There is considerable evidence that electronic transport is a dominant mechanism for the EC of plasma formed in strong shock waves in gases, including air mixtures. This indicates that, from a modeling point of view, the plasma formed behind normal shock waves in hypersonic and hypervelocity flows of air at speeds of practical interest (M_1 up to 30) can be treated as a low temperature plasma (LTP)—broadly defined as a plasma with electron energies on the order of the ionization

potential of atoms and molecules. Indeed, the LTP is a good approximation when the gas temperature is below 10^4 K (~1 eV). For air this is the case if $M_1 \lesssim 30$. In LTP, the EC is due to the transport of free e^- with a negligible contribution from the ionic conductivity. The dominant ionization reactions that produce free e^- in the shocked air are discussed in Section 3.1 and in Lin and Teare.[2] In Taylor,[14] the computational framework to calculate σ of the LTP was implemented, which is based on ab initio electronic structure methods and the Green-Kubo (GK) relation, and applied to high melting explosive (HMX) detonation products. However, the DC σ, which corresponds to zero frequency $\omega = 0$, cannot be directly computed using the GK expression and must be obtained by extrapolating the low-frequency GK values $\sigma(\omega)$ to zero. A powerful theoretical approach to obtain electronic transport properties of the LTP is based on the Boltzmann kinetic theory of charged test particles (electron swarm) in a neutral gas in the presence of an electric field.[15] In the Boltzmann kinetic theory, electrons are represented by the one-electron phase space distribution function $f(\mathbf{r}, \mathbf{v}, t)$, where $\mathbf{r}$, $\mathbf{v}$ are electron position and velocity coordinates and electron-atom interactions treated as collisions. The two most popular approaches for obtaining $f(\mathbf{r}, \mathbf{v}, t)$ are through solving the Boltzmann kinetic equation (BKE)[15–17] [or simply Boltzmann equation (BE)] and using the Monte Carlo collision (MCC) method.[18–20] In the hydrodynamic approximation,[15,17] σ is determined by the density (number of charged particles per unit volume), n, of e^- and transport properties of the e^- swarm (Eqs. 1–3). As the equilibrium ionization level and hence the n behind hypersonic and hypervelocity shock waves in the air are quickly reached, the n can be obtained independently, using free-energy calculations with available plasma thermochemical models using an accurate EOS.[21] The latter approach, in addition to being computationally less costly, has the advantage because it enables the ready achievement of consistency between chemical composition of the shocked gas and n.

In the present report we calculated the DC σ of dry air in hypersonic and hypervelocity flows at a pressure of 1 mm Hg and normal temperature (298 K) for the Mach numbers M_1 from 6 to 30 (2–10 km s^{-1}). The equilibrium thermodynamics of air plasma formed by neutrals, ions, and e^- was treated with the thermochemical computer code Cheetah 9.0,[22,23] while the e^- swarm transport coefficients were obtained under hydrodynamic conditions using the multiterm BE (MT-BE)[17,24] method and selectively benchmarked using the computationally more expensive MCC method.[20,25] Our results are compared to shock-tube experiments and theoretical predictions by Lamb and Lin,[11] and Lin et al.[10]

2. Computational Methods

For the conditions of interest, the shock-heated air is considered to be weakly ionized, $n << N$. The validity of this approximation is confirmed experimentally and theoretically.[2,3,10,11] In the present work, a weak ionization of the air plasma at $M_1 \le 30$ is further affirmed using equilibrium thermochemical and MCC calculations. In a weakly ionized plasma, the collisionality of the plasma species is dominated by scatterings from neutrals. Consequently, in the LTP at the kinetic theory level and *the hydrodynamic conditions* reviewed in Section 2.2, the σ, which relates the density of Ohmic e^- current

$$\mathbf{J}(\mathbf{r}) = \sigma \mathbf{E}(\mathbf{r}) \tag{1}$$

to the applied electric field $\mathbf{E}(\mathbf{r})$, is determined by the density n and e^- mobility μ:

$$\sigma = n\mu . \tag{2}$$

The mobility μ is related to the electron bulk drift velocity $\mathbf{W}$, one of the most important electron swarm parameters (which are bulk transport coefficients and reaction rates),[15,26]

$$\mu = \frac{W}{E} \tag{3}$$

where $W = |\mathbf{W}|$, $E = |\mathbf{E}|$. The theoretical e^- swarm parameters can be obtained using BE solvers or MCC approaches coupled with the hydrodynamic conditions. Application of the BE and MCC methods requires a knowledge of chemical composition $\{Y_{S,2}\}, n_2$ at the thermodynamic conditions behind the normal shock wave. These data can be obtained either from theoretical (e.g., ab initio or thermochemical EOS) calculations or experiment. In principle, the equilibrium n and ionization level can be obtained using the MCC simulation; however, in general this approach may not lead to an equilibrium with respect to the $\{Y_{S,2}\}$ and n_2 while additionally it is computationally expensive. A more consistent way is to use the thermochemical EOS calculations in which the model free energy function of the plasma is minimized with respect to concentrations $\{Y_S\}$ of ions, neutrals, and n. For the normal shock wave, the plasma EOS must be coupled with the equations arising from Rankine-Hugoniot jump conditions reviewed next in Section 2.1.

2.1 Normal Shock-Wave Thermodynamics

Notations used for a normal shock wave formed in the front of a hypersonic vehicle are shown in Fig. 1. As the thermodynamic equilibrium conditions are essentially reached in the upstream (labeled as $i=1$) and downstream (labeled as $i=2$) zones of the wave at a given shock velocity U_s, the corresponding states that are described by p_i, T_i, ρ_i, h_i, $\{Y_{S,i}\}$, n_i, must satisfy the Rankine-Hugoniot jump conditions. From these conditions, the following equations can be obtained

$$\frac{p_2 - p_1}{\rho_2^{-1} - \rho_1^{-1}} = -j^2 \tag{4}$$

where the mass flux $j \equiv \rho_1 u_1 = \rho_2 u_2$, and

$$h_2 - h_1 = 0.5\left(p_2 - p_1\right)\left(\rho_2^{-1} + \rho_1^{-1}\right) . \tag{5}$$

Equation 4 in the $p-\rho^{-1}$ plane is called the Raleigh line and Eq. 5 is termed the Hugoniot equation. To complete the description of the thermodynamics, we need to specify the material EOS $f_{EOS}\left(p,T,\rho,\{Y_S\},n\right)=0$ to relate the thermodynamic states across the shock front,

$$f_{EOS}\left(p_1,T_1,\rho_1,\{Y_{S,1}\},n_1\right) = f_{EOS}\left(p_2,T_2,\rho_2,\{Y_{S,2}\},n_2\right) = 0 , \tag{6}$$

and caloric EOS $h\left(p,\rho,\{Y_S\},n\right)$. The state p_2, T_2, ρ_2, $\{Y_{S,2}\}$, n_2, for a given shock Mach number $M_1 = u_1/a_1 = U_s/a_1$, and p_1, T_1, ρ_1, $\{Y_{S,1}\}$, ($n_1 = 0$) are a solution of Eqs. 4–6. More discussion on how to solve these equations for real air can be found in Wittliff and Curtis.[27] Inclusion of n into the Rankine-Hugoniot jump condition for energy (which stems from energy conservation at the shock front) is important for air plasma at $M_1 > 27$ when the energy invested in ionization is not small compared with the enthalpy of the shock-heated air. The n was not included into the energy conservation in many previous theoretical considerations.

2.2 Electron Transport in the Air Plasma: Kinetic Theory and Hydrodynamic Conditions

Under hydrodynamic conditions,[15] the one-electron distribution function $f\left(\mathbf{r},\mathbf{v},t\right)$ may be expanded with respect to the gradients of the free e^- density $n\left(\mathbf{r},t\right)$

$$f\left(\mathbf{r},\mathbf{v},t\right) = f^{(0)}\left(\mathbf{v}\right)n\left(\mathbf{r},t\right) - \boldsymbol{f}^{(1)}\left(\mathbf{v}\right)\bullet\nabla n\left(\mathbf{r},t\right) + \hat{f}^{(2)}\left(\mathbf{v}\right):\nabla\nabla n\left(\mathbf{r},t\right). \tag{7}$$

Similar expansions can be obtained for the flux $\mathbf{\Gamma}(\mathbf{r},t) = \mathbf{v}n(\mathbf{r},t)$ and the source term $S(\mathbf{r},t)$ in the continuity equation, which then adopts the form of the generalized diffusion equation

$$\frac{\partial n(\mathbf{r},t)}{\partial t} + \mathbf{W}\nabla n(\mathbf{r},t) - \hat{D} : \nabla\nabla n(\mathbf{r},t) = R_a n(\mathbf{r},t) \tag{8}$$

where the coefficients are the *bulk* swarm parameters: $\mathbf{W}$ (drift velocity), $\hat{D}$ (diffusion tensor), R_a (net ionization frequency). The bulk transport coefficients $\mathbf{W}$, $\hat{D}$ can be associated with the dynamics of the e^- swarm's center of mass.[15] By far, the most widely used kinetic treatments are based on solving the two-term[28,29] or more general MT-BE,[16,17] reviewed in Section 2.3, and on the MCC[20,25,30] method. Both the MT-BE and MCC approaches treat the e^--neutral interactions as collision processes described by the differential cross section $\sigma_{S,k}(\varepsilon)$ where *S* denotes a type of neutral specie and *k* denotes a type of collision (elastic, inelastic, and attachment). For this study, only isotropic scattering (when $\sigma_{S,k}$ become functions of electron kinetic energy ε) is accounted for. The elastic collisions utilize the conservative momentum transfer cross section $\sigma_{S,el}$, and similarly the inelastic collisions leading either to excitations or to ionizations with the process cross sections given by $\sigma_{S,exc}$ and $\sigma_{S,ioniz}$, respectively. The attachment processes are described by $\sigma_{S,att}$. The major source of the cross sections is the LXCat database:[31] an open-access platform for curating data needed to model the electron and ion components of the LTP.

2.3 MT-BE and MCC Methods

There are three main experimental setups[15,30,32,33] to determine the e^- swarm parameters. The setup used in the presented MT-BE (and benchmark MCC) calculations corresponds to time-of-flight (ToF) experiments in which behavior of the electrons in an isolated e^- swarm in free space (with the electrodes not taken into consideration) is studied. For the ToF experiments, the hydrodynamic conditions are satisfied such that the $f(\mathbf{r},\mathbf{v},t)$ may be decomposed into a series of velocity distribution functions, each corresponding to their respective order gradient in the electron density[15] (Eq. 7).

The MT-BE method involves solving the MT-BE in the hydrodynamic approximation. This formulation is based on the transport theory comprehensively detailed by Kumar et al.[15] In the absence of a magnetic field, the BE can be written as

$$\frac{\partial f}{\partial t}+\mathbf{v}\frac{\partial f}{\partial \mathbf{r}}+\frac{e}{m_e}\mathbf{E}\frac{\partial f}{\partial \mathbf{v}}=-C\left[f\right] \tag{9}$$

where e, m_e are charge and mass of the electron in the swarm, which can be inhomogeneous and time dependent, and $-C\left[f\right]$ denotes the linear e^--neutral collision integral. With an appropriate collision term $C\left[f\right]$, the BE equation can be used to describe almost all nonrelativistic problems that arise in plasma physics. The hydrodynamic approximation is invoked by substituting Eq. 7 into Eq. 9 and then solving it for the coefficients of the *k*th ($k=0,1,2$) density gradient. This leads to a system of coupled equations for $f^{(0)}\left(\mathbf{v}\right)$, $\boldsymbol{f}^{(1)}\left(\mathbf{v}\right)$, $\hat{f}^{(2)}\left(\mathbf{v}\right)$. Assuming that the electrical field $\mathbf{E}$ is uniform and *z*-directed, the bulk drift velocity $\mathbf{W}$ has only one component W_z in the *z*-direction and the diffusion tensor $\hat{D}$ is taken to be symmetric with a longitudinal component D_L along the *z*-direction. The following expressions for the swarm parameters

$$R_a=\int C\left[f^{(0)}\left(\mathbf{v}\right)\right]d\mathbf{v}\ , \tag{10}$$

$$W_z=\int v_z f^{(0)}\left(\mathbf{v}\right)d\mathbf{v}+\int C\left[f_z^{(1)}\left(\mathbf{v}\right)\right]d\mathbf{v}\ , \tag{11}$$

$$ND_L=\int v_z f_z^{(1)}\left(\mathbf{v}\right)d\mathbf{v}+\int C\left[f_{zz}^{(2)}\left(\mathbf{v}\right)\right]d\mathbf{v} \tag{12}$$

where $v=\left|\mathbf{v}\right|$, $\mathbf{v}=\left(v_x,v_y,v_z\right)$, can be obtained. The terms containing the collision operator $C\left[\cdot\right]$ describe the source/sink contributions to the bulk transport.

A common strategy for solving the BE is to expand the $f^{(0)}\left(\mathbf{v}\right)$, $\boldsymbol{f}^{(1)}\left(\mathbf{v}\right)$, $\hat{f}^{(2)}\left(\mathbf{v}\right)$ into a truncated series of orthogonal functional bases (spherical harmonics, Legendre polynomials, etc.). The common choice is Legendre polynomials, $\left\{P_l\left(\cos\vartheta\right)\right\}_{l=0}^{N_l-1}$, where $\cos\vartheta=v_z/v$. Expanding these functions in terms of Legendre polynomials results in a comparatively simple system of equations to be solved. For example, we have for

$$f^{(0)}\left(\mathbf{v}\right)=\sum_{l=0}^{N_l-1}f_l^{(0)}\left(v\right)P_l\left(\cos\theta\right)\ . \tag{13}$$

Similar expansions can be written for $\boldsymbol{f}^{(1)}\left(\mathbf{v}\right)$ and $\hat{f}^{(2)}\left(\mathbf{v}\right)$. Using these expansions, a set of N_l coupled differential equations can be derived[17,26] for $f_l^{(0)}\left(v\right)$, $\boldsymbol{f}_l^{(1)}\left(v\right)$, and $\hat{f}_l^{(2)}\left(v\right)$. In most cases, a relatively small number of Legendre polynomials ($N_l=4-10$) are needed to achieve satisfactory convergence of the solution $f\left(\mathbf{v}\right)$. By far, the most widely applied tool to achieve

this is the application of a two-term BE model when $N_l = 2$. The MT-BE models arise if $N_l > 2$. Once the solutions $f_l^{(0)}(v)$, $\boldsymbol{f}_l^{(1)}(v)$, and $\hat{f}_l^{(2)}(v)$ are obtained, the transport coefficients in Eqs. 10–12 can be calculated. The drift velocity $W = W_z$ is used to calculate the EC σ in accordance with Eqs. 2 and 3.

It is convenient to write down the equations for $f_l^{(0)}(\varepsilon)$, $\boldsymbol{f}_l^{(1)}(\varepsilon)$, and $\hat{f}_l^{(2)}(\varepsilon)$ using the electron energy $\varepsilon = mv^2/2$ as an independent variable instead of v.[17] The $f_0^{(0)}(\varepsilon)$ is the electron energy distribution function (EEDF), which is normalized as $\int \varepsilon^{1/2} f_0^{(0)}(\varepsilon)\, d\varepsilon = 1$. The mean electron energy is then

$$\langle \varepsilon \rangle = \int \varepsilon^{3/2} f_0^{(0)}(\varepsilon)\, d\varepsilon . \tag{14}$$

The collision integral $C[f]$ is the sum of terms describing collisions of different kinds. Derivations of each of the collision terms is described in detail in Loureiro and Amorim.[26] To solve the differential equations for $f_l^{(0)}(\varepsilon)$, $\boldsymbol{f}_l^{(1)}(\varepsilon)$, and $\hat{f}_l^{(2)}(\varepsilon)$, a finite difference scheme is employed.

The two-term ($N_l = 2$) BE approach is generally appropriate in situations where scattering collisions are frequent enough to keep the angular distribution close to an isotropic distribution and the anisotropy is so small that it is sufficient to keep just the first two low-order terms in the spherical harmonic expansion. The MT-BE solvers provide better accuracy and, as discussed in the literature,[29] are mandatory for all gases whenever the accuracy $\leq 0.1-1\%$ of the swarm parameters is required; the two-term BE is generally sufficient for low accuracy ($\geq 10\%$) plasma applications. The described MT-BE framework is implemented in the MultiBolt computer code,[17] which we utilized in our calculations.

In the MCC method, the e^- swarm is represented by the set of N_e electrons (typically N_e is in the range $1\times10^5 - 1\times10^6$), which undergo collisions with background-neutral particles with the collision probability estimated using the Monte Carlo method.[20,25] The bulk transport coefficients are determined by time-averaging the trajectories $\{\boldsymbol{r}_i(t)\}_{i=1}^{N_e}$ of the individual e^- in the swarm (Fig. 2). Additional details on the implementation of conservative and nonconservative collisions and on the data sampling used to calculate averages are given in Rabie and Franck.[1] The MCC method is free from approximations introduced by a use of finite N_l in MT-BE solver; however, it is computationally more expensive. In this work, we benchmarked several selected properties of air plasma using the MCC calculations carried out with the METHES computer code.[20]

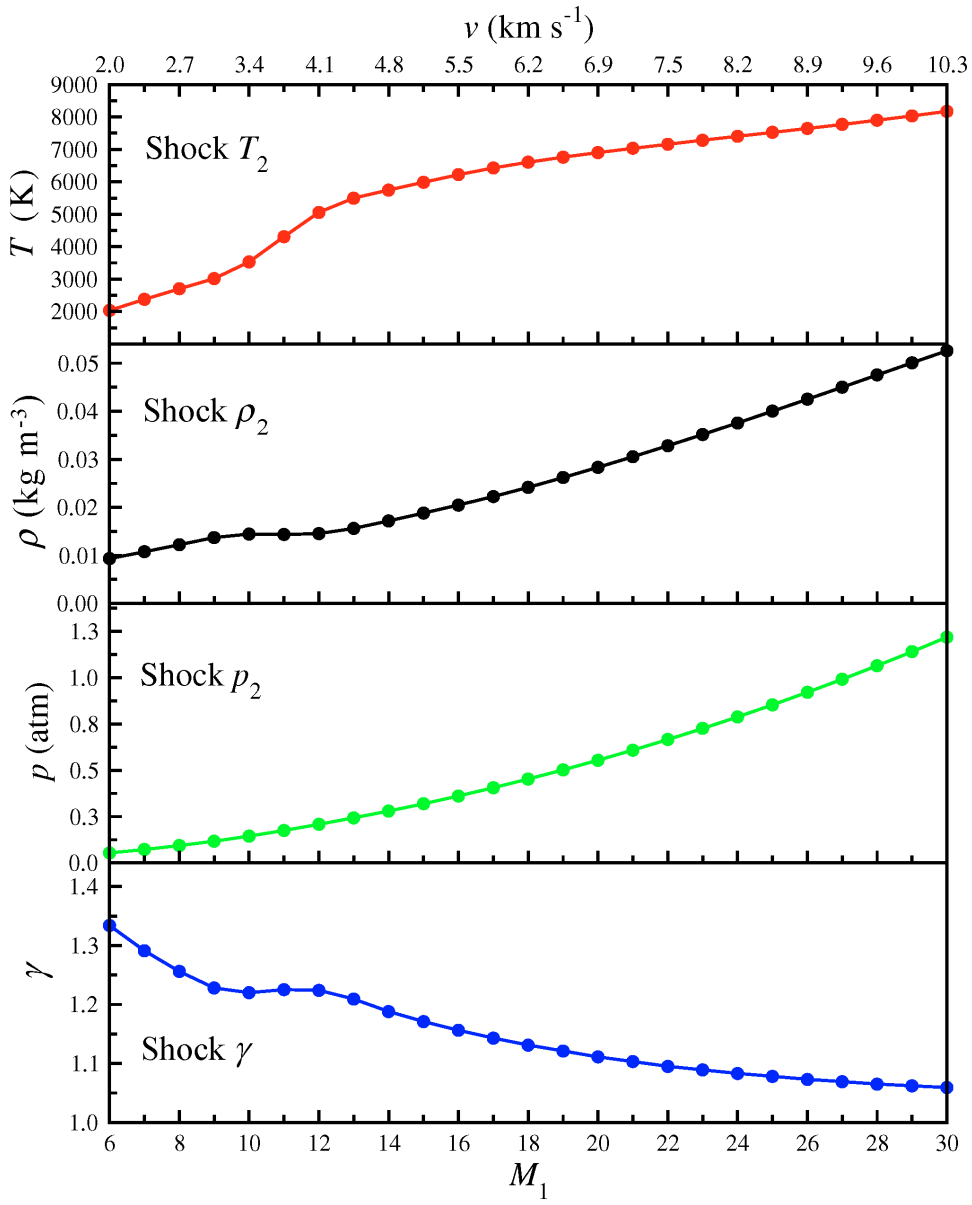

Fig. 2 **Equilibrium temperature T_2, density ρ_2, and pressure p_2, and specific heat capacity ratio $\gamma = c_p / c_V$ behind the normal shock wave as functions of shock Mach number M_1. Initial pressure $p_1 = 0.001316$ atm (1 mm Hg), density $\rho_1 = 0.001559$ kg m^{-3} (Note: NTP $\rho = 1.204$ kg m^{-3}), and temperature $T_1 = 298$ K.**

3. Results and Discussion

3.1 Chemical Composition of Dry Air Plasma and Free Electron Density Behind a Normal Shock Wave

In the present work, for each M_1, the state p_2, T_2, ρ_2, $\{Y_{S,2}\}$, n_2 ($n = n_2 N$) of shocked air (Fig. 1, zone 2) was determined by solving Eqs. 4–6 using the thermochemical equilibrium model and ionic Exp6 EOS product library as implemented in the Cheetah 9.0 code.[22,23] This method consistently accounts for the contribution from dissociation and ionization reactions into the Hugoniot curve. The undisturbed air mixture (Fig. 1, zone 1) was considered to be a trietary mixture consisting of 78% of N_2, 21% of O_2, and 1% of Ar, that is, $\{Y_{N_2,1}, Y_{O_2,1}, Y_{Ar,1}\} = \{0.78, 0.21, 0.01\}$ (inclusion of CO_2, and other minor constituents would only complicate the computations without contributing much to the essential results). For the shocked air plasma (Fig. 1, zone 2), in addition to neutrals (listed in Table 1), the following ionic species were included in the calculations: N^+, O^+, O^-, N_2^+, O_2^+, N_2^-, O_2^-, O_3^+, NO^+, and e^-. Typical compositions of the shocked air at several M_1 are compiled in Table 1. A dependence of the shocked thermodynamic state p_2, T_2, ρ_2, and heat capacity ratio $\gamma = c_p / c_V$ on M_1 are shown in Fig. 2. The temperature of the shock-heated gas, T_2, remains well below 10^4 K for the entire studied range of M_1 justifying use of the LTP model. The mole fractions $\{Y_{S,2}\}$ of individual chemical species and ions are presented in Fig. 3, and the corresponding e^- density is displayed in Fig. 4. For $M_1 = 8 - 20$, these results agree well overall with those reported by Lamb and Lin.[11] The Hugoniot T_2 obtained in our work is somewhat higher than that reported by Lamb and Lin,[11] lower than that compiled in Zeldovich and Raizer,[34] and agrees with theoretical Hugoniot data presented in Wittliff and Curtis.[27] The differences are due to variations in dissociation and ionization mechanisms included in the models. However, as we demonstrate, the thermal ionization rate and resulting e^- density predicated by Cheetah 9.0 Exp6 EOS leads to good agreement between the theoretical and experimental σ. Note, the concentration of e^- by Cheetah 9.0 (and hence the σ) are sensitive (by a factor of several) to the variations in T_2 within the range of differences between the aforementioned Hugoniot calculations.

Table 1 **Mole fraction composition of air plasma behind the normal shock wave at several values of shock Mach number M_1 using the Cheetah 9.0 Exp6 EOS methodology. The mole fraction of Ar[a] remains constant (0.01) and is not shown. The corresponding p_2, T_2, and ρ_2 are given in Fig. 2. Each footnote next to the species name references the LXCat cross section database.[31]**

M_1	N_2[a]	O_2[a]	N[b]	O[b]	NO[c]	NO_2[d]	N_2O[e]	O_3[f]	Ions
8	0.712	0.110	4.42×10^{-5}	0.132	0.0361	3.77×10^{-6}	5.23×10^{-7}	1.54×10^{-8}	6.56×10^{-10}
20	0.154	1.65×10^{-5}	0.594	0.239	1.53×10^{-3}	1.23×10^{-9}	3.65×10^{-8}	1.44×10^{-11}	9.49×10^{-4}
30	0.0291	6.56×10^{-6}	0.740	0.212	5.25×10^{-4}	3.68×10^{-10}	1.07×10^{-8}	1.39×10^{-11}	4.42×10^{-3}

[a]Biagi-v8.97 database[19]
[b]IST-Lisbon database[35]
[c]Itikawa database[36,37]
[d]Quantemol database: electron collision cross sections were generated using the Quantemol-N[38] implementation of the UK Molecular R-matrix computer code (UKRMol)[39]
[e]Hayashi database[40]
[f]W Lowell Morgan, Kinema Research Software database

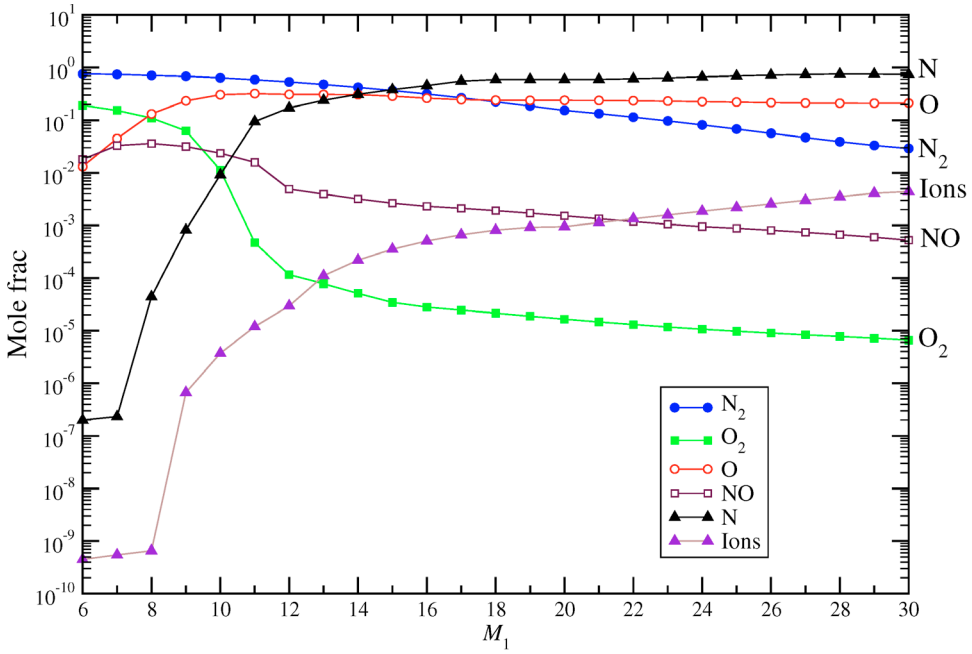

Fig. 3 **Air plasma composition (in mole fractions) behind a normal shock wave as a function of shock Mach number M_1 for the same p_1, T_1, ρ_1 as in Fig. 2. The mole fraction of Ar is constant (0.01) and is not shown.**

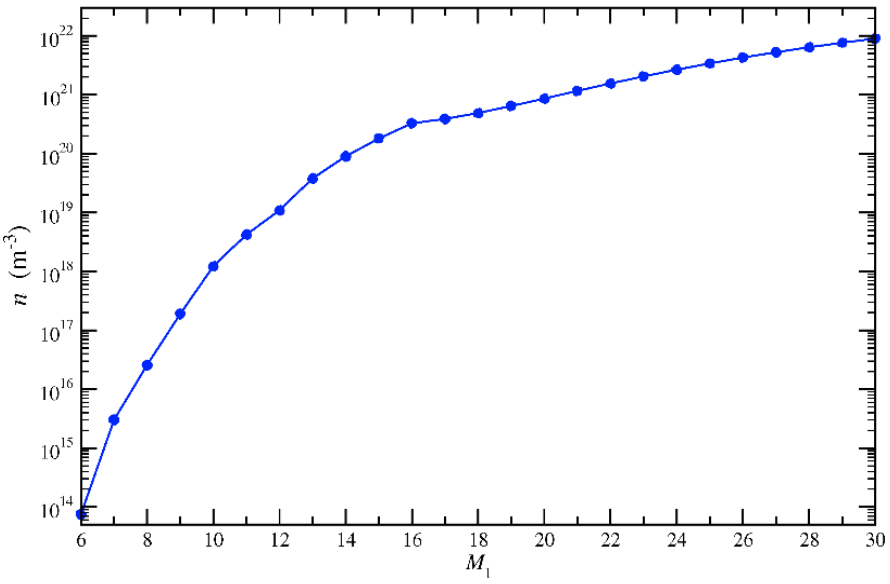

Fig. 4 Equilibrium free electron density n behind a normal shock wave as a function of shock Mach number M_1 for the same p_1, T_1, ρ_1 (as in Fig. 2)

The air at the front of the shock wave starts to notably dissociate at about $M_1 = 8-9$ (Fig. 3). A sharp decrease—by almost three orders of magnitude—in the concentration of O_2 is observed as the M_1 increases from 9 to 13, while the concentration of N_2 decreases fairly steadily over the entire range of M_1 studied here, with a notable pickup in the rate of dissociation at around $M_1 = 13$. As seen from Fig. 2, the M_1 within the 9–13 range is characterized by a much faster increase in the T_2 while the $\rho_2(M_1)$ and $\gamma(M_1)$ are nearly flat.

It was concluded that for M_1 up to 27, the predominant mechanism is AI through $N + O + 2.8\text{eV} \rightarrow NO^+ + e^-$ (this reaction has the lowest ionization energy).[2] For higher M_1, the electron impact reactions $e^- + M \rightarrow M^+ + 2e^-$, which have considerably higher potentials, become a dominant ionization mechanism while the AI additionally proceeds through $N + N + 5.8\text{eV} \rightarrow N_2^+ + e^-$, and possibly $N + O_2 + 6.5\text{eV} \rightarrow NO_2^+ + e^-$, and $O + O + 6.9\text{eV} \rightarrow O_2^+ + e^-$ channels.[2,3] The dominance of the AI mechanism through $N + O$ collisions agrees with the theoretical data presented in Figs. 3 and 4. Specifically, for $M_1 \geq 9$, the change in the concentration of NO, O_2, N_2 correlates inversely with the change in the concentration of ions and e^-. Furthermore, because for stronger shocks the reactions $N + N \rightarrow N_2^+ + e^-$, $N + O_2 \rightarrow NO_2^+ + e^-$, $O + O \rightarrow O_2^+ + e^-$ become more important as a source of equilibrium e^-, for larger M_1, the correlation between the N, O concentrations and the n becomes increasingly complex.

3.2 Electron Transport Properties of Shock-Heated Air

The remaining property necessary to calculate the σ (Eq. 2) is the mobility μ, which is related to the bulk drift velocity $\mathbf{W}$, one of the transport coefficients of the e^- swarm (see Eqs. 11 and 12). The full set of transport coefficients was determined using the MT-BE and MCC models as described in Section 2.3. The set of cross sections $\{\sigma_{S,el}, \sigma_{S,exc}, \sigma_{S,ioniz}, \sigma_{S,att}\}$ for the species in the air plasma formed under shock-wave compression were obtained from the LXCat database.[31] The data sets are detailed in Table 1. In spite of some significant differences in the details of the individual cross sections, most of these data sets yield swarm parameters in good agreement with the experiments.[41] Several cross sections are plotted in Fig. 5. The MT-BE model simulations are based on the framework of the MultiBolt computer code.[17,24] The size of the Legendre basis was selected as $N_l = 4$. A larger N_l does not lead to meaningful changes in the simulated plasma transport properties.

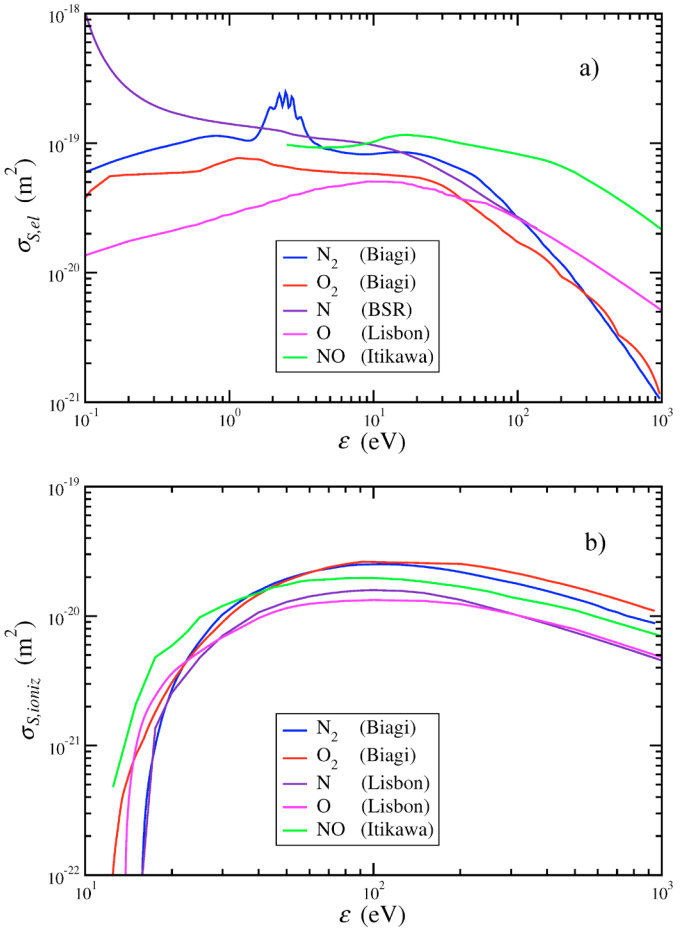

Fig. 5 Elastic-momentum transfer cross sections $\sigma_{S,el}(\varepsilon)$: a) and ionization cross sections $\sigma_{S,ioniz}(\varepsilon)$; b) for the most abundant species in shock-heated dry air (see Table 1)

For $M_1 \le 20$, it was demonstrated that the maximum ∇n behind a normal shock wave appears to vary with the ρ_2^2, indicating that all the important rate-governing steps are due to binary collisions.[10] However, at higher M_1, the higher-order collisions could be important. The calculated MT-BE EEDFs are displayed in Fig. 6. The EEDFs are in good agreement with those calculated using the MCC method. The distinct advantage of the MT-BE calculations is an absence of numerical noise clearly observed in the MCC solutions. The mean electron energy $\langle \varepsilon \rangle$ (Eq. 14) from the MT-BE model is presented in Fig. 7. The EEDF $f_0^{(0)}(\varepsilon)$ versus M_1 undergoes most pronounced changes at ε within the $2.0-6.2$ eV range. This further supports the earlier observation that the AI reactions $\mathrm{N}+\mathrm{O} \rightarrow \mathrm{NO}^+ + e^-$ and $\mathrm{N}+\mathrm{N} \rightarrow \mathrm{N}_2^+ + e^-$ are the prevailing mechanism for the ionization in the range of M_1 studied here. The total ionization rate R_a as a function of E/N is shown in Fig. 8. The bulk drift velocity $\mathbf{W}$, which has only one component in the z-direction $W_z = W$ (Eq. 11) is displayed in Fig. 9 and the bulk longitudinal diffusion coefficient, neutral density product $D_L N$ versus E/N is given in Fig. 10.

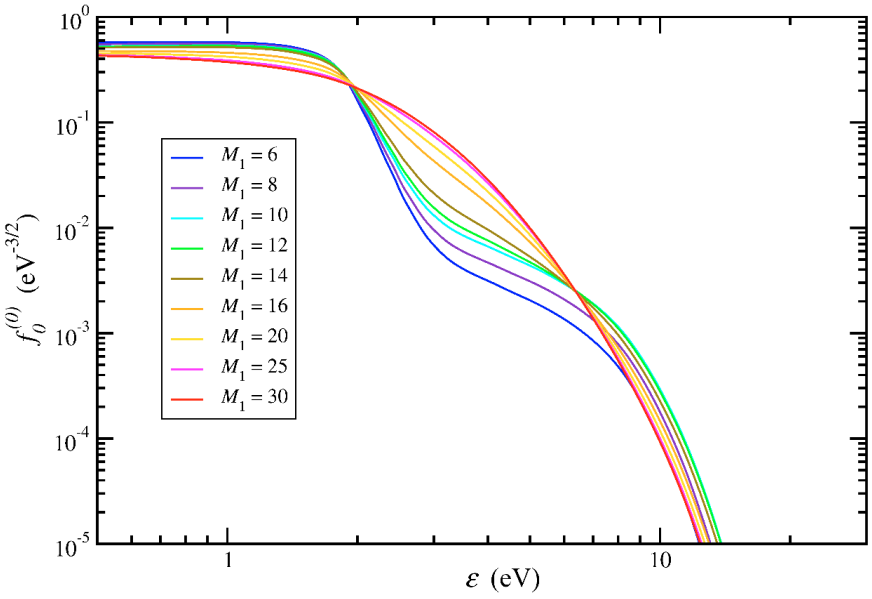

Fig. 6 EEDF $f_0^{(0)}(\varepsilon)$ for different shock Mach numbers M_1 as predicted by the MT-BE model

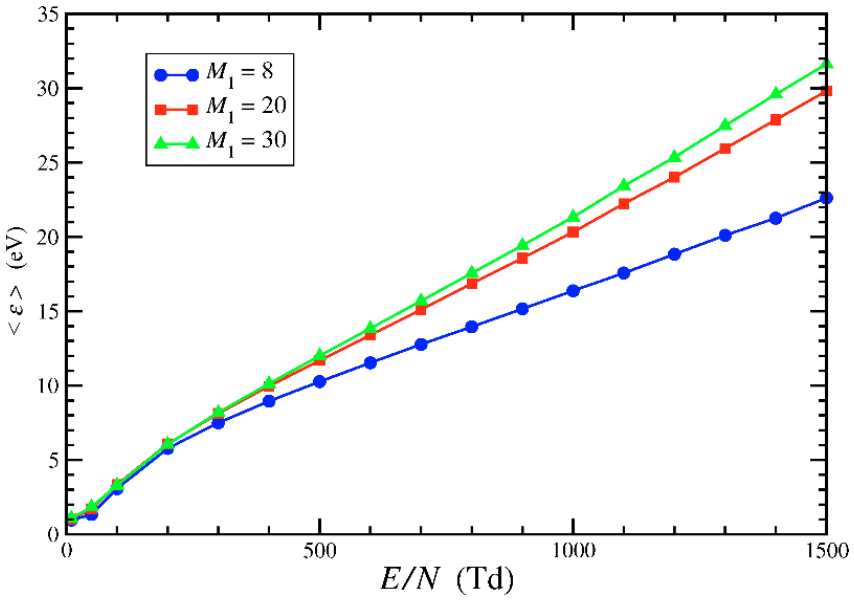

Fig. 7 **Mean electron energy $\langle \varepsilon \rangle$ vs. reduced electric field E/N for selected shock Mach numbers M_1 as predicted by the MT-BE model**

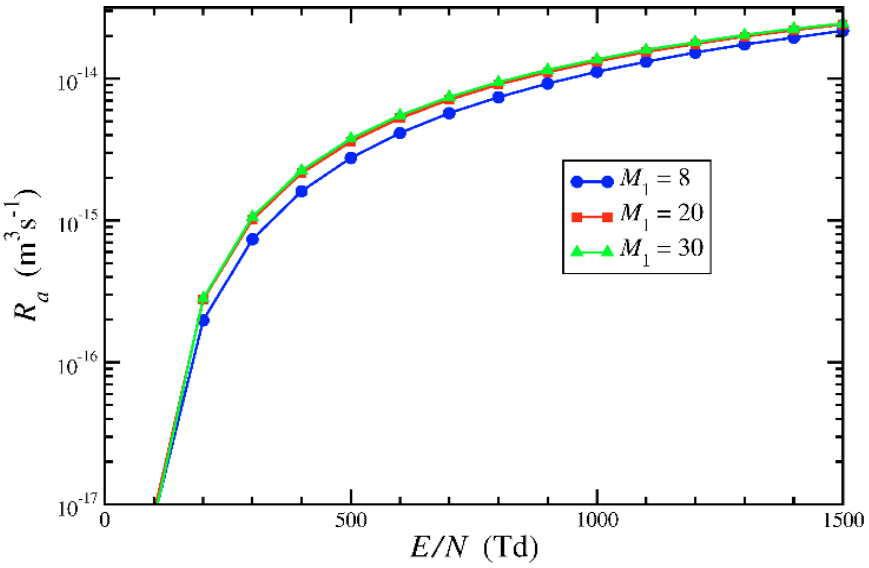

Fig. 8 **Ionization rate R_a vs. reduced electric field E/N for selected shock Mach numbers M_1 as predicted by the MT-BE model**

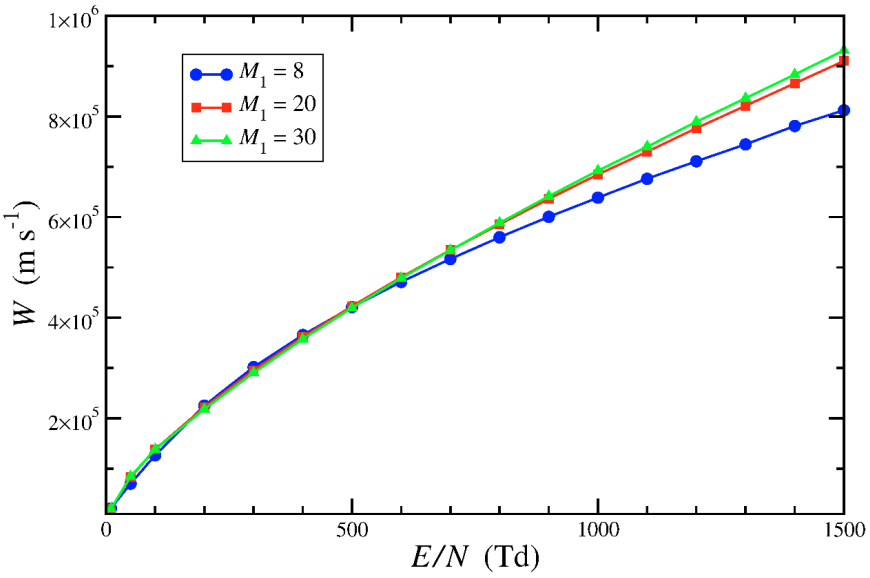

Fig. 9 Bulk drift velocity W vs. reduced electric field E/N for selected shock Mach numbers M_1 as predicted by the MT-BE model

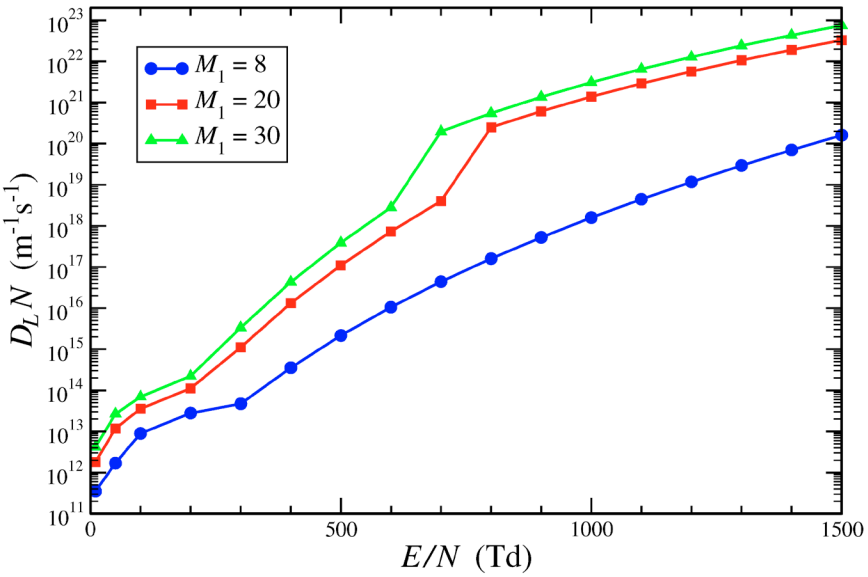

Fig. 10 Bulk longitudinal diffusion coefficient $D_L N$ vs. reduced electric field E/N for selected shock Mach numbers M_1 as predicted by the MT-BE model

The $\langle \varepsilon \rangle$ and bulk transport coefficients versus reduced electric field E/N curves shift upward more notably when M_1 is increased from 8 to 20 compared to when the M_1 varies in the $20-30$ range despite ρ_2 increasing more in the latter range of M_1. This is an effect of the diminishing role of the variations in the plasma composition on the transport properties with increasing M_1 when $M_1 > 20$ (see Fig. 3).

3.3 Electron Conductivity

We now connect the aforementioned calculations to determine the EC σ of the air plasma (Fig. 1, zone 2) as a function of shock Mach number M_1. Recall that the σ was determined from Eq. 2. The required electron mobility μ was calculated from Eq. 3 using the bulk drift velocity W from the MT-BE calculations (Eq. 11) (similar results for W were obtained using the MCC method). The W versus E/N from the ME-BE calculations is shown in Fig. 9. The EC was calculated using the W taken at $E/N = 50$ Td when the W versus E/N is close to linear.

The calculated $\sigma(M_1)$ using the Cheetah 9.0 Exp6 EOS (n in Eq. 2) and MT-BE (μ in Eq. 2) method is shown in Fig. 9. The $\sigma(M_1)$ appears in excellent agreement with the shock-tube experiments by Lamb and Lin[11] carried out in the range of $10 \le M_1 \le 18$. This points to the validity of our major assumption that the shock-compressed plasma is close to equilibrium. The range of M_1 can be fragmented roughly into three parts: $M_1 \le 10$; $10 < M_1 \le 27$; and $M_1 > 27$. For $M_1 \le 10$, the σ is low, on the order of σ observed in detonation products of most high explosives[7] (0.1 S m^{-1}). The growth of σ with increasing M_1 is driven mostly by the dissociation of O_2 and formation of NO (see Fig. 3). The AI reaction $N + O \rightarrow NO^+ + e^-$ becomes a major source of equilibrium e^- in the range of $10 < M_1 \le 27$. The other three AI reactions $N + N \rightarrow N_2^+ + e^-$, $N + O_2 \rightarrow NO_2^+ + e^-$, and $O + O \rightarrow O_2^+ + e^-$ (which are slower than $N + O \rightarrow NO^+ + e^-$ at low T_2 but quickly accelerate at higher T_2) gradually contribute more to the equilibrium n and hence to the σ. In this region, the σ increases by two orders of magnitude. For $M_1 > 27$, the ionization mechanism becomes dominated by electron-neutral impacts and perhaps the kinetic methods are better suited to calculate the EC in this range. The rate of increase of $\sigma(M_1)$ with M_1 grows, for example, $\sigma'(M_1 = 10) = 1$ S m^{-1} Ma^{-1}, $\sigma'(20) = 37$ S m^{-1} Ma^{-1}, and $\sigma'(30) = 84$ S m^{-1} Ma^{-1}.

The use of equilibrium n corresponds to the infinitely fast dissociation model. For large M_1, the finite reaction rates lead to the ionization level and hence σ being dependent on distance to the shock front. For example, as discussed in the literature,[3] the $N + O$ collision becomes the rate-limiting step in the ionization for $M_1 \ge 23$ as the ionization increasingly involves faster channels through charge exchange; consequently, ionization by this means leads to an increase in the ionization distance (to the shock front). The distance-dependent $\sigma(M_1)$ can, in principle, be obtained using kinetic approaches to model the time evolution of the plasma composition and ionization behind the shock front, for example, using the kinetic Monte Carlo method, which can be combined with the MCC method.

Compiling these efforts, Fig. 11 illustrates the EC of shocked air as a function of shock Mach number or, equivalently, velocity (v). Confidence in these results are well-validated by the experimental data of Lamb and Lin.[11] We are unaware of any experimental data above 6 km s^{-1}; therefore, these results provide important data for validating and enhancing hydrocode EC models. Up to hypersonic shock speeds (~5 km s^{-1}), there is an enormous growth in air EC by six orders of magnitude. Its growth slows considerably such that, between 5–10 km s^{-1}, EC only increases by a factor of 10.

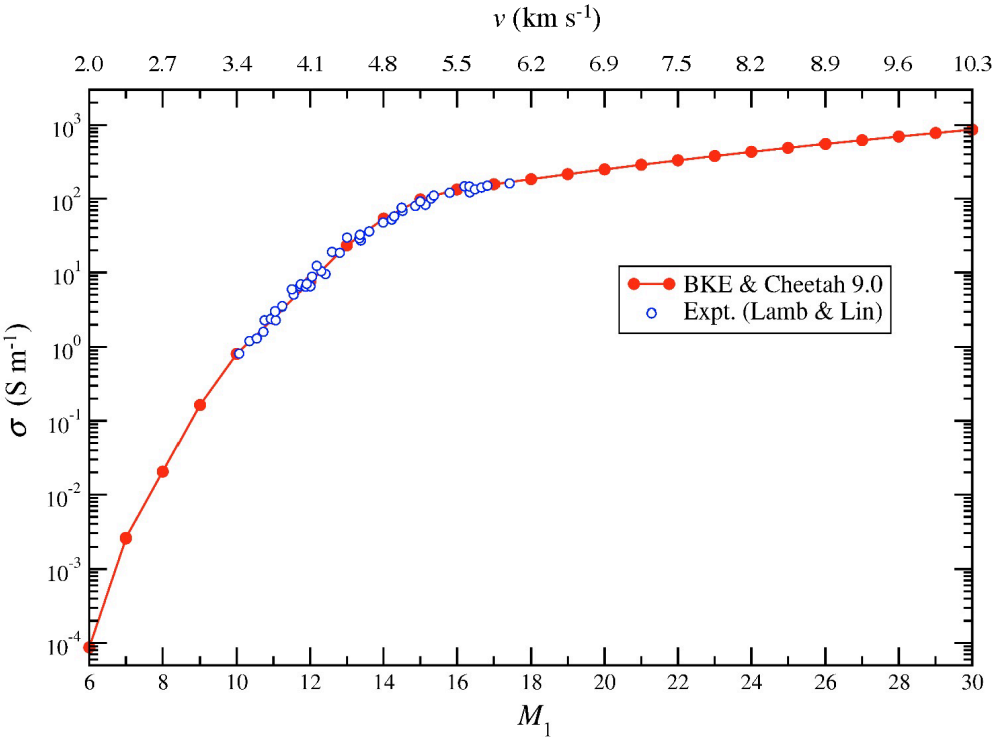

Fig. 11 The EC σ of shocked (dry) air vs. shock Mach number M_1 as predicted by the MT-BE and Cheetah 9.0 Exp6 EOS methods

The BKE and Cheetah 9.0 data can be conveniently fit to a functional form. Figure 12 illustrates this using MATLAB's curve-fitting toolbox and a two-term exponential function for $\log_{10}\sigma$, such that

$$\sigma(v) = 10^{[a\exp(bv)+c\exp(dv)]} \tag{15}$$

where $a = 2.427, b = 0.01752, c = -26.07, d = -0.6891$. These parameters are based on v using units of km s^{-1} rather than SI units since shock speeds are typically of this order. The quality of this fit is supported by $R^2 = 0.9983$ with tight 95% confidence bounds and a root mean square error of 0.8. The model is not appropriate however as $v \to 0$, where the ambient dry air EC value is about 10^{-14} S m^{-1}. We would expect other mechanisms to take over in approaching this limit.

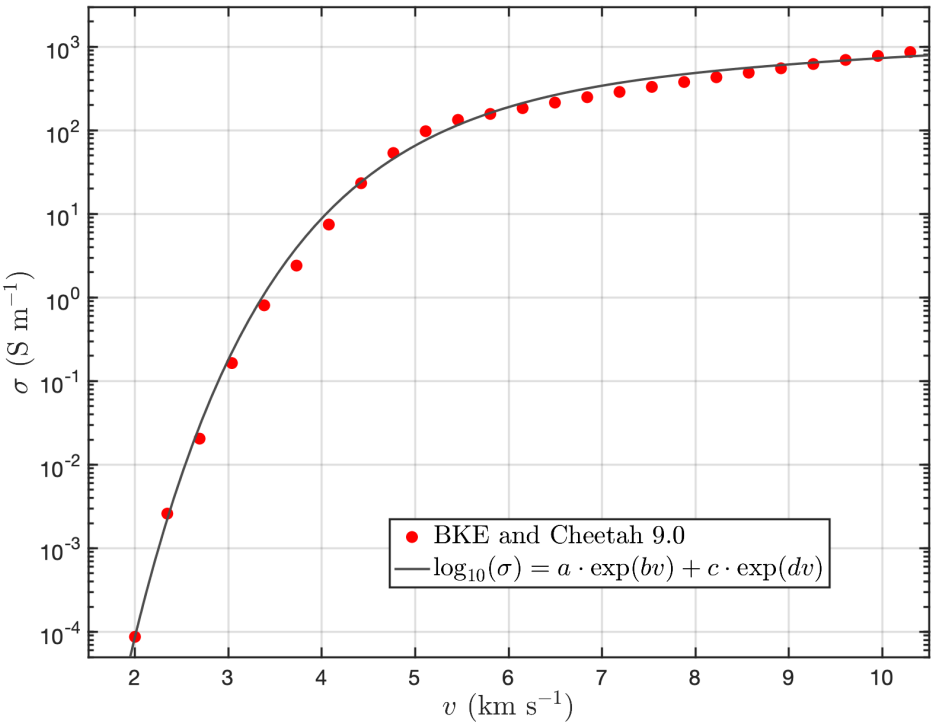

Fig. 12 Comparison of theoretical $\sigma(M_1)$ in Fig. 11 and its numerical fit using model in Eq. 15

4. Conclusions

We theoretically studied the DC EC of the plasma produced in normal shock waves in hypersonic flows of dry air for shock Mach numbers M_1 in the range of 6–30 (about 2.0–10.3 km s^{-1}). The thermodynamic conditions, chemical composition, and free electron density of the shock-compressed plasma were determined using the thermochemical equilibrium model and ionic Exp6 EOS product library as implemented in Cheetah 9.0. The calculated thermodynamic properties clearly justify a treatment of the plasma formed behind the shock wave as the weakly ionized LTP in the entire range of M_1 studied here. Consequently, the electronic transport properties were simulated in the framework of MT-BE methods and benchmarked using the MCC method. The MT-BE calculations employed the MultiBolt computer code and the MCC simulations were carried out using the METHES code. The MT-BE and MCC calculations are based on the cross-section sets available from the open-source LXCat database. We then evaluated the EC $\sigma(M_1)$ and compared it with existing experimental and theoretical data. The obtained $\sigma(M_1)$ agrees well with the shock-tube experiments, which were for a narrower range of M_1. The analysis of the thermochemical and transport properties indicate that the AI mechanism through $\mathrm{N+O}$ collisions and through $\mathrm{N+N}$

collisions at higher M_1 is the dominant ionization mechanism. Kinetic methods such as kinetic Monte Carlo and MCC can be used to sample a spatial distribution of the plasma composition and free electron density behind the shock wave that becomes important to accurately estimate $\sigma(M_1)$ for $M_1 \geq 27$.

The theoretical calculations presented here demonstrate that the EC of the air behind normal shock waves for shock Mach numbers up to 30 can be modeled in the context of equilibrium thermokinetics and transport of a homogeneous LTP. Particularly, an accurate equilibrium procedure for determination of Hugoniot states (i.e., that based on the Cheetah 9.0 EOS) in combination with the Boltzmann kinetic equation or Monte Carlo collision methods (with available accurate cross sections for electron-neutral collisions to determine charge transport properties of the air LTP) is able to predict the shock-tube measurements by Lamb and Lin.[11] This supports the validity of the framework for stronger shocks as long as an assumption of the LTP in thermochemical equilibrium is valid. For stronger shocks, the predictive calculations may require combining the equilibrium methods with kinetic approaches to model off-equilibrium evolution of the chemical composition, charge density, and the electronic transport as well as considering the contribution to the EC from the ionic species.

We quantified the EC of shocked (dry) air as a function of shock Mach number or, equivalently, velocity (v). Confidence in these results are well-validated by the experimental data of Lamb and Lin.[11] We are unaware of any experimental data above 6 km s^{-1}; therefore, these results provide important data for validating and enhancing hydrocode EC models. Additionally, the approaches used here and subsequent results can be used to develop a functional form of $\sigma(M_1)$, such as one presented herein, for utilization by other modeling codes.

5. References

1. Anderson JD. Hypersonic and high-temperature gas dynamics. American Institute of Aeronautics and Astronautics; 2006.
2. Lin SC, Teare JD. Rate of ionization behind shock waves in air. 2. Theoretical interpretations. Phys Fluids. 1963;6(3):355–375.
3. Wilson J. Ionization rate of air behind high-speed shock waves. Phys Fluids. 1966;9(10):1913–1921.
4. Sasoh A. Compressible fluid dynamics and shock waves. Springer; 2020.
5. Hayes B. On the electrical conductivity in detonation products. Proc. 4th Symp. (Int.) on Detonation; 1967. p. 595–601. Office of Naval Research.
6. Ershov AP, Satonkina NP. Investigation of the reaction zone in heterogeneous explosives substances using an electrical conductivity method. Combust Explos. 2009;45(2):205–210.
7. Izvekov S, Doney RL. Modeling of electrical conductivity of detonation products in octahydro-1,3,5,7-tetranitro-1,3,5,7-tetrazocine (HMX). Army Research Laboratory (US); 2021. Report No.: ARL-TR-9232.
8. Edwards DH, Hooper G, Collyer AA. Ionization measurement in reactive shock and detonation waves using microwave techniques. J Phys D Appl Phys. 1971;4(6):854–868.
9. In: Brun RE, editor. High Temperature Phenomena in Shock Waves. Shock Wave Science and Technology Reference Library. Springer; 2014 July.
10. Lin SC, Neal RA, Fyfe WI. Rate of ionization behind shock waves in air.1. Experimental results. Phys Fluids 1962;5(12):1633–1648.
11. Lamb L, Lin SC. Electrical conductivity of thermally ionized air produced in a shock tube. J Appl Phys. 1957;28(7):754–759.
12. Boyd ID. Modeling of associative ionization reactions in hypersonic rarefied flows. Phys Fluids. 2007;19(9):096102–10.
13. Boyd ID, Josyula E. Analysis of associative ionization rates for hypersonic flows. J Thermophys Heat Transf. 2021;35(3):484–493.
14. Taylor DE. ECON-KG: A code for computation of electrical conductivity using density functional theory. Army Research Laboratory (US); 2017. Report No.: ARL-TR-8196.

15. Kumar K, Skullerud HR, Robson RE. Kinetic-theory of charged-particle swarms in neutral gases. Aust J Phys. 1980;33(2B):343–448.

16. Petrovic ZL, Dujko S, Maric D, Malovic G, Nikitovic Z, Sasic O, Jovanovic J, Stojanovic V, Radmilovic-Radenovic M. Measurement and interpretation of swarm parameters and their application in plasma modelling. J Phys D Appl Phys. 2009;42(19):194002–33.

17. Stephens J. A multi-term Boltzmann equation benchmark of electron-argon cross-sections for use in low temperature plasma models. J Phys D Appl Phys. 2018;51(12):125203–11.

18. Lucas J, Saelee HT. A comparison of a Monte Carlo simulation and Boltzmann solution for electron swarm motion in gases. J Phys D Appl Phys. 1975;8(6):640–650.

19. Biagi SF. Monte Carlo simulation of electron drift and diffusion in counting gases under the influence of electric and magnetic fields. Nucl Instrum Methods Phys Res Sect A Accel Spectrom Dect Assoc Equip. 1999;421(1–2):234–240.

20. Rabie M, Franck CM. METHES: A Monte Carlo collision code for the simulation of electron transport in low temperature plasmas. Comput Phys Commun. 2016;203:268–277.

21. Redmer R. Physical properties of dense, low-temperature plasmas. Phys Rep Rev Sec Phys Lett. 1997;282(2–3):35–157.

22. Fried L, Souers P. CHEETAH: A next generation thermochemical code. Lawrence Livermore National Laboratory; 1994. Report No.: UCRL-ID-117240.

23. Bastea S, Fried LE, Glaesemann KR, Howard WM, Kuo I-FW, Nimmakayala S, Souers PC, Taller D, Vitello PA. Cheetah 9.0 User's manual. Energetic Materials Center. Lawrence Livermore National Laboratory; 2019.

24. Stephens JC. A multi-term, multi-harmonic Boltzmann equation model for kinetic behavior in intense microwave and terahertz excited low temperature plasmas. Phys Plasmas. 2018;25(10):103502–10.

25. Thomas RWL, Thomas WRL. Monte Carlo simulation of electrical discharges in gases. J Phys B At Mol Phys. 1969;2(5):562–570.

26. Loureiro J, Amorim J. Kinetics and spectroscopy of low temperature plasmas. Springer; 2016.

27. Wittliff CE, Curtis JT. Normal shock wave parameters in equilibrium air. Cornell Aeronautical Lab Inc; 1961. Report No.: AD0270202.

28. Lin SL, Robson RE, Mason EA. Moment theory of electron-drift and diffusion in neutral gases in an electrostatic-field. J Chem Phys. 1979;71(8):3483–3498.

29. White RD, Robson RE, Schmidt B, Morrison MA. Is the classical two-term approximation of electron kinetic theory satisfactory for swarms and plasmas? J Phys D Appl Phys. 2003;36(24):3125–3131.

30. Sakai Y, Sakamoto S, Tagashira H. Variation of steady-state electron mean energy between parallel plates in argon. J Phys B At Mol Phys. 1972;5(5):1010–1016.

31. CDAP database. [accessed 2020 July 10]. www.lxcat.net.

32. Robson RE. Transport phenomena in the presence of reactions: Definition and measurement of transport coefficients. Aust J Phys. 1991;44(6):685–692.

33. Dujko S, White RD, Petrovic ZL. Monte Carlo studies of non-conservative electron transport in the steady-state Townsend experiment. J Phys D Appl Phys. 2008;41(24):245205–11.

34. Zeldovich YB, Raizer YP. Physics of shock waves and high temperature hydrodynamic phenomena. Academic Press; 1966. Vol. I.

35. Alves LL. The IST-LISBON database on LXCat. J Phys Conf Ser. 2014;565(1):012007.

36. Itikawa Y, Mason N. Cross sections for electron collisions with water molecules. J Phys. Chem. Ref. Data 2005;34(1):1–22.

37. Itikawa, Y. Cross sections for electron collisions with carbon monoxide. J Phys Chem Ref Data. 2015;44(1):013105–17.

38. Tennyson J, Brown DB, Munro JJ, Rozum I, Varambhia HN, Vinci N. Quantemol-N: an expert system for performing electron molecule collision calculations using the R-matrix method. 5th EU-Japan Symposium on Plasma Processing; 2007; Belgrade, Serbia. IOP Publishing Ltd.

39. Carr JM, Galiatsatos PG, Gorfinkiel JD, Harvey AG, Lysaght MA, Madden D, Masin Z, Plummer M, Tennyson J, Varambhia HN. UKRmol: a low-energy electron- and positron-molecule scattering suite. Eur Phys J D. 2012;66(3): 58–11.

40. Hayashi M. Bibliography of electron and photon cross sections with atoms and molecules published in the 20th century - Argon. National Institute for Fusion Science of Japan; 2003. Report No.: NIFS-DATA--72. www.nifs.ac.jp/report/nifs-data072.html.

41. Pitchford LC, Alves LL, Bartschat K, Biagi SF, Bordage MC, Phelps AV, Ferreira CM, Hagelaar GJM, Morgan WL, Pancheshnyi S, et al. Comparisons of sets of electron-neutral scattering cross sections and swarm parameters in noble gases: I. Argon. J Phys D Appl Phys. 2013;46(33):334001–19.

List of Symbols, Abbreviations, and Acronyms

AI	associative ionization
BE	Boltzmann equation
BKE	Boltzmann kinetic equation
DC	direct current
DEVCOM	US Army Combat Capabilities Development Command
DOD	Department of Defense
EC	electrical conductivity
EEDF	electron energy distribution function
EOS	equation of state
GK	Green-Kubo
HMX	high melting explosive
LTP	low temperature plasma
MCC	Monte Carlo collision
MT-BE	multiterm Boltzmann equation
NTP	normal temperature pressure
SI	International System of Units
ToF	time-of-flight

1 (PDF) DEFENSE TECHNICAL INFORMATION CTR DTIC OCA

1 (PDF) DEVCOM ARL FCDD RLD DCI TECH LIB

2 (PDF) FOI - SWEDEN P APPELGREN P LUNDBERG

1 (PDF) LLNL A JOHNSON

14 (PDF) DEVCOM ARL FCDD RLW WA S IZVEKOV FCDD RLW TC J CAZAMIAS FCDD RLW TD R DONEY B KRZEWINSKI M ZELLNER FCDD RLW TA P BERNING S BILYK M COPPINGER M GRINFELD C UHLIG FCDD RLW TE D HORNBAKER C KRAUTHAUSER P SWOBODA G VUNNI

11 (PDF) SANDIA NATL LAB S BOVA J CARPENTER K COCHRANE M DESJARLAIS T FULLER J NIEDERHAUS C O'BRIEN A PORWITZKY A ROBINSON C SIEFERT J WILKES